



HAL
open science

Activation of Nod2 signalling upon Norovirus infection enhances antiviral immunity and susceptibility to colitis

Ghaffar Muharram, Marion Thépaut, Pierre-Emmanuel Lobert, Teddy Grandjean, Olivier Boulard, Myriam Delacre, Emmrich Wakeford, Richard Wheeler, Lionel Franz Poulin, Ivo Gomperts Boneca, et al.

► To cite this version:

Ghaffar Muharram, Marion Thépaut, Pierre-Emmanuel Lobert, Teddy Grandjean, Olivier Boulard, et al.. Activation of Nod2 signalling upon Norovirus infection enhances antiviral immunity and susceptibility to colitis. *Gut microbes*, 2023, 10.1080/19490976.2023.2249960 . hal-04101382v3

HAL Id: hal-04101382

<https://hal.science/hal-04101382v3>

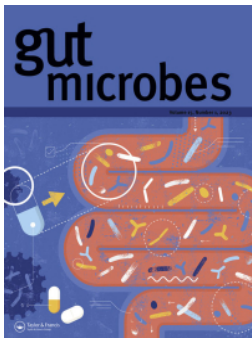
Submitted on 30 Oct 2023

HAL is a multi-disciplinary open access archive for the deposit and dissemination of scientific research documents, whether they are published or not. The documents may come from teaching and research institutions in France or abroad, or from public or private research centers.

L'archive ouverte pluridisciplinaire **HAL**, est destinée au dépôt et à la diffusion de documents scientifiques de niveau recherche, publiés ou non, émanant des établissements d'enseignement et de recherche français ou étrangers, des laboratoires publics ou privés.



Distributed under a Creative Commons Attribution - NonCommercial 4.0 International License



Activation of Nod2 signaling upon norovirus infection enhances antiviral immunity and susceptibility to colitis

Ghaffar Muharram, Marion Thépaut, Pierre-Emmanuel Lobert, Teddy Grandjean, Olivier Boulard, Myriam Delacre, Emmrich Wakeford, Richard Wheeler, Lionel Franz Poulin, Ivo Gomperts Boneca, Frank Lafont, Marie-Cécile Michallet, Didier Hober, Ken Cadwell & Mathias Chamailard

To cite this article: Ghaffar Muharram, Marion Thépaut, Pierre-Emmanuel Lobert, Teddy Grandjean, Olivier Boulard, Myriam Delacre, Emmrich Wakeford, Richard Wheeler, Lionel Franz Poulin, Ivo Gomperts Boneca, Frank Lafont, Marie-Cécile Michallet, Didier Hober, Ken Cadwell & Mathias Chamailard (2023) Activation of Nod2 signaling upon norovirus infection enhances antiviral immunity and susceptibility to colitis, Gut Microbes, 15:2, 2249960, DOI: [10.1080/19490976.2023.2249960](https://doi.org/10.1080/19490976.2023.2249960)

To link to this article: <https://doi.org/10.1080/19490976.2023.2249960>



© 2023 The Author(s). Published with license by Taylor & Francis Group, LLC.



[View supplementary material](#)



Published online: 01 Sep 2023.



[Submit your article to this journal](#)



Article views: 396



[View related articles](#)



[View Crossmark data](#)

Activation of Nod2 signaling upon norovirus infection enhances antiviral immunity and susceptibility to colitis

Ghaffar Muharram^a, Marion Thépaut^a, Pierre-Emmanuel Lobert^c, Teddy Grandjean^a, Olivier Boulard^b, Myriam Delacre^a, Emmrich Wakeford^a, Richard Wheeler^e, Lionel Franz Poulin^b, Ivo Gomperts Boneca^e, Frank Lafont^a, Marie-Cécile Michallet^d, Didier Hober^c, Ken Cadwell^{f,g,h}, and Mathias Chamaillard^b

^aUniv. Lille, CNRS, Inserm, CHU Lille, Institut Pasteur de Lille, Lille, U1019 - UMR 9017 - CIL - Centre d'Infection et d'Immunité de Lille, Lille, France; ^bLaboratory of Cell Physiology, INSERM U1003, University of Lille, Lille, France; ^cUniv Lille, Faculté de Médecine, CHU Lille, Laboratoire de Virologie ULR3610, Lille, France; ^dTERI (Tumor Escape, Resistance and Immunity), Centre de recherche en cancérologie de Lyon, Centre Léon Bérard, Université de Lyon, Université Claude Bernard Lyon 1, Inserm 1052, CNRS 5286, Lyon, France; ^eInstitut Pasteur, Université Paris Cité CNRS UMR6047, INSERM U1306, Unité de Biologie et génétique de la paroi bactérienne, Paris, France; ^fKimmel Center for Biology and Medicine at the Skirball Institute, New York University Grossman School of Medicine, New York, NY, USA; ^gDepartment of Microbiology, New York University Grossman School of Medicine, New York, NY, USA; ^hDivision of Gastroenterology and Hepatology, Department of Medicine, New York University Langone Health, New York, NY, USA

ABSTRACT

Over 90% of epidemic non-bacterial gastroenteritis are caused by human noroviruses (NoVs), which persist in a substantial subset of people allowing their spread worldwide. This has led to a significant number of endemic cases and up to 70,000 children deaths in developing countries. NoVs are primarily transmitted through the fecal-oral route. To date, studies have focused on the influence of the gut microbiota on enteric viral clearance by mucosal immunity. In this study, the use of mouse norovirus S99 (MNoV_S99) and CR6 (MNoV_CR6), two persistent strains, allowed us to provide evidence that the norovirus-induced exacerbation of colitis severity relied on bacterial sensing by nucleotide-binding oligomerization domain 2 (Nod2). Consequently, *Nod2*-deficient mice showed reduced levels of gravity of Dextran sodium sulfate (DSS)-induced colitis with both viral strains. And MNoV_CR6 viremia was heightened in *Nod2*^{-/-} mice in comparison with animals hypomorphic for *Atg16l1*, which are prone to aggravated inflammation under DSS. Accordingly, the infection of macrophages derived from WT mice promoted the phosphorylation of Signal Transducer and Activator of Transcription 1 (STAT1) and NOD2's expression levels. Higher secretion of Tumor Necrosis Factor alpha (TNFα) following NOD2 activation and better viral clearance were measured in these cells. By contrast, reduced levels of pSTAT1 and blunted downstream secretion of TNFα were found in *Nod2*-deficient macrophages infected by MNoV_S99. Hence, our results uncover a previously unidentified virus-host-bacterial interplay that may represent a novel therapeutic target for treating noroviral origin gastroenteritis that may be linked with susceptibility to several common illnesses such as Crohn's disease.

ARTICLE HISTORY

Received 23 May 2023
Revised 13 August 2023
Accepted 16 August 2023





KEYWORDS

Antiviral immunity; colitis; macrophages NOD2; norovirus; signaling


Introduction

The development of high throughput sequencing techniques progressively helped us gain a better comprehension of the composition of the enteric virome.¹ This is of particular importance for unraveling how some enteric viruses can establish persistent infections and subsequently influence our health.^{2,3} Among these, noroviruses (NoVs) have been studied for several years. These single stranded RNA (+) viruses, belonging to the family of *Caliciviridae*, are responsible for the majority of non-bacterial

gastroenteritis worldwide. Until recent progress in cultivation methods of noroviruses from genogroups I, II, IV, VIII, and IX⁴⁻⁶ that infect humans (HuNoVs), mechanistic details were mostly obtained from studies using the mouse norovirus (MNoV).⁷ Indeed, MNoVs can be easily produced *in vitro* in macrophages or dendritic cells.⁸ Several MNoV strains have been described based on their shedding time in the stool and classified as either persistent or acute (non-persistent) strains.⁹ Owing to the variety

CONTACT Mathias Chamaillard  mathias.chamaillard@inserm.fr  Faculté de Médecine, CHU Lille, Laboratoire de Virologie, Univ. Lille, Lille, France; Ghaffar Muharram  ghaffar.muhammad@pasteur-lille.fr  CIL - Centre d'Infection et d'Immunité de Lille, Universities Lille, CNRS, Inserm, CHU Lille, Institut Pasteur de Lille, U1019 - UMR 9017, Lille F-59000, France

This article has been corrected with minor changes. These changes do not impact the academic content of the article.

 Supplemental data for this article can be accessed online at <https://doi.org/10.1080/19490976.2023.2249960>

© 2023 The Author(s). Published with license by Taylor & Francis Group, LLC.

This is an Open Access article distributed under the terms of the Creative Commons Attribution-NonCommercial License (<http://creativecommons.org/licenses/by-nc/4.0/>), which permits unrestricted non-commercial use, distribution, and reproduction in any medium, provided the original work is properly cited. The terms on which this article has been published allow the posting of the Accepted Manuscript in a repository by the author(s) or with their consent.

of circulating NoV strains, strain-dependent effects are expected to occur and should be studied in more details. Even a single amino acid change in the NS1/2 viral protein is sufficient to switch the acute MNoV_CW3 strain to a persistent state,¹⁰ showing the high degree of adaptability of NoV genomes and hence their versatility to counteract host defense mechanisms. Type III interferon (IFN- λ) response has been shown to control the *in vivo* propagation of the persistent MNoV_CR6 strain,¹¹ while type I and II interferons mediate innate immune responses against acute MNoV infections.^{12,13}

Multiple intracellular pattern recognition receptors (PRRs) have been associated with indirect noroviral detection, especially during NoV genome replication, when double stranded RNA intermediates are generated.¹⁴ As such, the Toll-like receptor 3 (TLR3) that recognizes any dsRNA in the endosomal compartment and the melanoma differentiation associated protein-5 (MDA-5), a member of the RIG-I-like receptor (RLR) family that recognizes long dsRNA, have been shown to participate in the detection of the MNoV_1 strain and its plaque isolate the MNoV_CW3.¹⁵ Among the Nod-like receptor (NLR) family, it was shown that the loss of Nlrp6 impairs antiviral immunity to MNoV_1.¹⁶ Besides its ability to sense muropeptides from Gram positive and negative bacteria,¹⁷ the nucleotide-binding oligomerization domain 2 (NOD2) was also shown to directly bind with the genome (ssRNA-) of the respiratory syncytial virus (RSV) to induce antiviral responses.¹⁸ The recruitment of MAVS by NOD2 was needed to activate the interferon-regulatory factor 3 (IRF3) dependent signaling and promote IFN- β production. In the same line, NOD2-dependent signaling was shown to disrupt intestinal homeostasis and increase lethality in an *E. Coli* and MNoV_1 co-infection mouse model.¹⁹

Another molecular player that is essential to activate antiviral signaling is the cytosolic protein signal transducer and activator of transcription 1 (STAT1). MNoV_1 infection was shown to be lethal in STAT1-deficient mice.¹² Furthermore, STAT1-dependent interferon responses were shown to limit MNoV_1 replication and dissemination *in vivo*.²⁰

Interestingly, Cadwell and colleagues have demonstrated how infection with the MNoV persistent strain CR6 rendered *Atg16l1^{HM}* mice more

susceptible to DSS-induced colitis.²¹ Interestingly, the interaction of NOD2 with ATG16L1 was shown to regulate the autophagy clearance of pathogenic bacteria.²² Furthermore, it has been established that loss-of-function point mutations of either *NOD2* or *ATG16L1* predispose humans to Crohn's disease.^{23,24} Insights into the mechanisms of how NOD2 signaling is regulated upon noroviral infection and whether it may subsequently modulate colitis susceptibility remained to be assessed.

In this study, we have investigated how NOD2 influences the pathogenesis of the two persistent murine norovirus strains MNoV_S99 (*Berlin*)²⁵ and MNoV_CR6 *in vivo* in DSS-induced colitis models. At the cellular level, the *Nod2*-dependent pro-inflammatory signaling pathway activation was further examined in response to MNoV_S99 and MNoV_CR6 infection in myeloid cells to determine how this in turn subsequently affects viral production.

Results

MNoV_S99 exacerbates the severity of DSS-induced inflammation

Since MNoV_S99 is a natural strain commonly found in animal facilities that is able to establish persistent infections,²⁵ we assessed the implication of MNoV_S99 in the exacerbation of colitis. Hence, we examined MNoV_S99's impact in a widely used chemically induced colitis model that is induced upon the administration of Dextran Sodium Sulfate (DSS). Specifically, C57BL/6J mice were first infected with a single dose of 5×10^7 TCID50/mL of MNoV_S99 or mock-treated with PBS (200 μ L). One week later, drinking water was replaced with either a 3% DSS or 5% DSS solution for a period of seven consecutive days (Figure 1a). Body weight-loss was monitored on a daily basis together with signs of diarrhea and rectal bleeding. With both concentrations of DSS, the pre-treatment with MNoV_S99 had induced a more significant body weight loss (purple and orange curves Figure 1b-c). After 7 d of DSS treatment, mice were euthanized and the disease severity was evaluated. Histological analysis of colon sections revealed an increased infiltration of inflammatory cells and more pronounced epithelial damages in

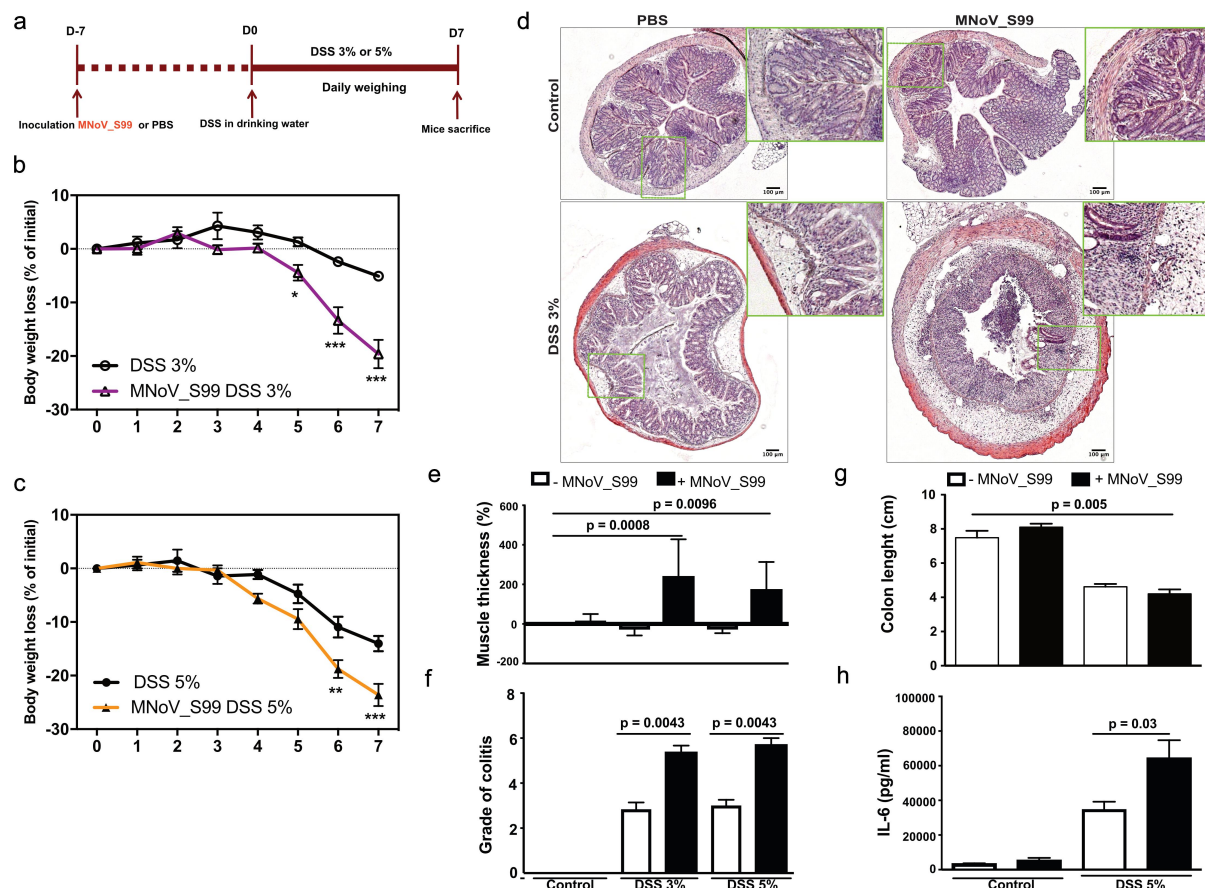


Figure 1. MNoV_S99 aggravates inflammation in DSS-induced colitis. a)- *in vivo* experimental design, C57BL/6J mice were orally gavaged with PBS (200 μ L) or MNoV_S99 (5×10^7 TCID₅₀/mL), 7 d later, all the mice were given DSS in drinking water for a week. Mice were weighed daily for weight loss comparison. b)- 3% DSS-induced colitis \pm MNoV_S99 (n = 6). c)- 5% DSS-induced colitis \pm MNoV_S99 (n = 6). In b) and c), statistical differences were determined by two-way ANOVA test, * $p < 0.05$, ** $p < 0.01$, *** $p < 0.001$. d)- Representative images from H&E staining of colon sections from mock-treated (control) or 3% DSS \pm MNoV_S99 treated mice. Insets showing higher magnifications from each image are presented next to each image. e)- muscle wall thickness was determined with image J from colon section images. Percentages of increase are plotted after baseline subtraction relative to the values obtained from control mice (n = 6). f)- histological intestinal epithelial inflammation scores comparison between control, 3% or 5% DSS \pm MNoV_S99 treated mice (n = 6). g)- colon length comparison between control and 5% DSS \pm MNoV_S99 treated mice h)- IL-6 secretion levels from colon explants from mock or 5% DSS \pm MNoV_S99 treated mice (n = 6). Statistical differences were determined with Student's *t*-test in E, F, G and H.

infected mice treated with DSS when compared to similarly challenged animals that were not infected (Figure 1d). Accordingly, increased muscle thickness was measured in colon sections from mice treated with the virus in the presence of both 3% and 5% DSS in comparison with mock-treated control mice (Figure 1e). Similarly, histological scoring of the hematoxylin and eosin (H&E) stained colonic sections expectedly showed significantly more severity in MNoV_S99-infected mice treated with either 3% or 5% DSS than DSS alone (Figure 1f). Upon mice sacrifice, resected colons were measured. A significantly reduced length

was obtained in mice infected with MNoV_S99 and treated with 5% DSS in comparison with non-infected control animals (PBS) (Figure 1g). The increased level of colitis was also evidenced by a significantly augmented secretion of the pro-inflammatory cytokine interleukin-6 (IL-6) in the supernatants of overnight *in vitro* cultured colon explants from MNoV_S99 infected +5% DSS treated mice versus those from DSS only mice (Figure 1h). Taken together, these data clearly show that MNoV_S99 infection is able to lower the resistance of mice to chemically induced colitis.

MNoV_S99-associated inflammation is abrogated in *Nod2*^{-/-} mice

In cells from the myeloid lineage, NOD2 was shown to participate in the sensing of *Citrobacter rodentium* and of commensal bacteria that are translocating in response to DSS-induced epithelial injury²⁶. To determine whether NOD2 is also implicated in the immunopathology associated with MNoV in our preclinical model of colitis, we compared the severity of DSS-induced colitis in the presence or absence of MNoV_S99 between WT and *Nod2*-deficient mice. In contrast to what was observed in WT mice (Figure 2a), the sensitizing effect of the virus on the daily weight-loss was absent upon MNoV_S99 infection of *Nod2*^{-/-} mice (Figure 2b). These data suggest that the pro-inflammatory effect of MNoV_S99 observed in WT mice may depend on the degree of bacterial sensing through NOD2.

Indeed, DSS induces an abrasion of the epithelial barrier allowing commensal bacteria to cross the mucosa and unleash a NOD2-dependent pro-inflammatory response. This was further confirmed after mice were autopsied. Colon tissue section staining showed decreased levels of colonic inflammation from MNoV_S99 infected *Nod2*^{-/-} vs WT mice (Figure 2c). In agreement, muscle thickness quantification from these colon sections showed significantly increased thickness in MNoV_S99-infected WT mice under 3% DSS treatment vs 3% DSS alone (Figure 2d). The variations of colon length measurements that were induced upon MNoV_S99 infection in WT mice were absent by contrast in *Nod2*^{-/-} mice (Fig. S1A). Similarly, differences in histological scores and mucosal wall thickness measured from MNoV_S99-infected WT mice vs DSS alone were also blunted in *Nod2*^{-/-} infected

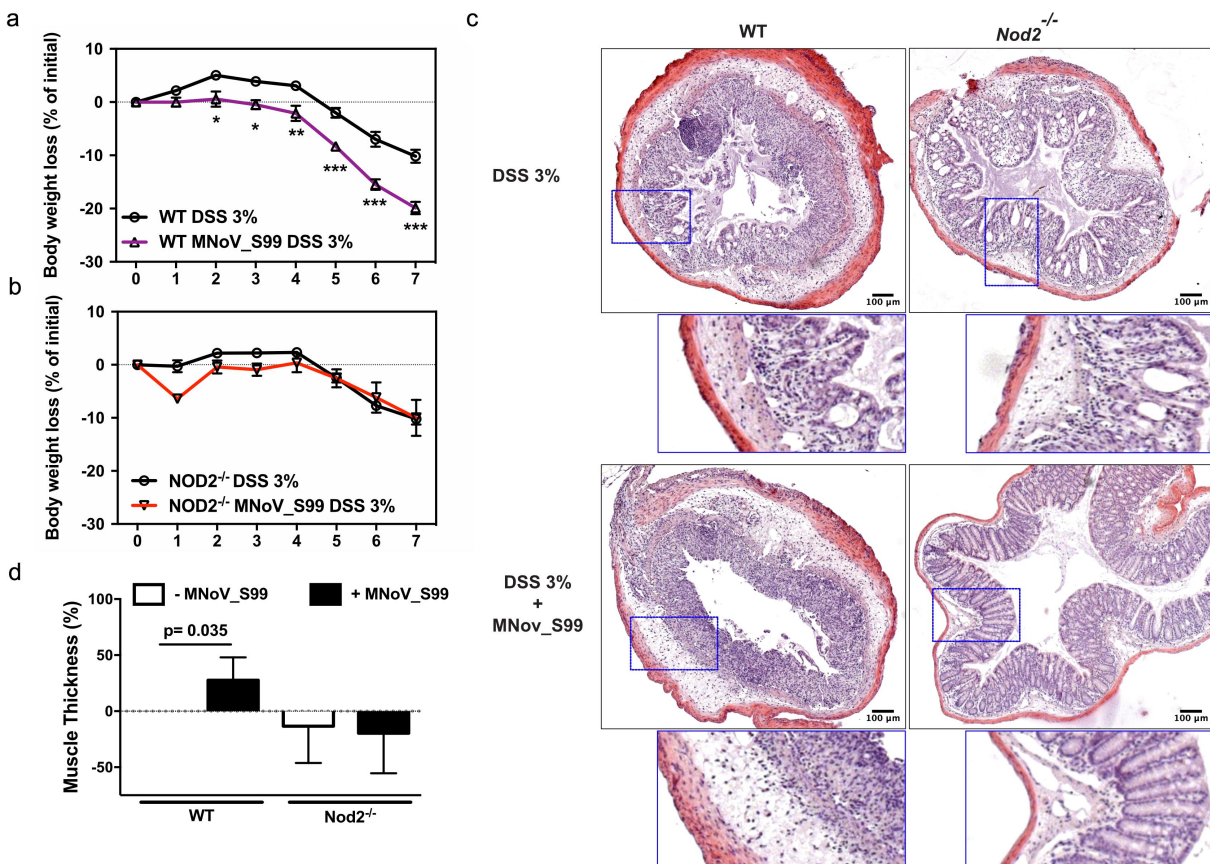


Figure 2. MNoV_S99-associated inflammation is NOD2 dependent weight loss comparison in a)- 3% DSS-induced colitis \pm MNoV_S99 in WT mice ($n = 6$) and b)- in *Nod2*^{-/-} mice ($n = 6$), statistical differences were determined by two-way ANOVA test, * $p < 0,05$, ** $p < 0,01$, *** $p < 0,001$. c)- Representative images of H&E staining of colon sections from mice in a) and b). Insets showing higher magnifications are presented below each image. d)- Percentages of increase of muscle wall thickness from colon section images are plotted after baseline subtraction relatively to the values obtained from WT mice treated only with DSS ($n = 6$), statistical differences were determined with Student's *t*-test.

mice (Fig. S1B). And a clear trend was observed regarding the increased levels of secretion of tumor necrosis factor α (TNF α) in the supernatants of *in vitro* cultured colon explants from WT mice infected with MNoV_S99 and treated with 3% DSS vs those with DSS only. This effect was absent in the supernatants from *Nod2*^{-/-} mice infected and treated similarly (Fig. S1C).

Overall, these data demonstrate that the excessive inflammatory response measured in the presence of MNoV_S99 depends on NOD2-dependent bacterial sensing in our DSS-induced colitis mouse model.

Mouse noroviruses infections trigger NOD2-dependent pro-inflammatory signaling

Mouse noroviruses are known to have a tropism for the myeloid cell lineages, namely macrophages and dendritic cells. Recently, it was shown that tuft cells belonging to the gut epithelial cellular lineages, that possess the CD300lf MNoV receptor can also be targeted by the MNoV_CR6 strain.²⁷

Making use of the GFP-Nod2 reporter mice line, we first examined in which cellular lineage Nod2 is expressed within the intestinal mucosa. We failed to observe any GFP-Nod2 expression in epithelial cells. By contrast, GFP signal was detectable in the bulk of the cells below the lamina propria where intestinal mononuclear phagocytes are primarily located (Figure 3a). Hence, the NOD2-dependent response to MNoV_S99 infection was further studied in macrophages, monocytes, and dendritic cells in our *in vitro* cellular models.

Interferon production being one of the most common responses to the intracellular presence of RNA genomes of foreign origin, we next examined if the STAT1 signaling pathway that lays upstream of ATG1611-mediated interferon production was activated in response to murine norovirus infection. To this end, bone marrow-derived macrophages (BMDM) from WT mice were infected with several persistent and non-persistent MNoV strains at a multiplicity of infection (Moi) of 1, for 1 h and the levels of overexpression of pSTAT1 from cell lysates were measured by western blot (Figure 3b). In contrast to the non-persistent strain MNoV_CW3 that caused a striking increase in pSTAT1 levels, infections with

the persistent strains S99 and CR6 induced a much milder STAT1 signaling pathway activation. The CW1 strain was associated with the lowest level of STAT1 activation.

Since MNoV_S99 is a natural strain commonly found in animal facilities that is able to establish persistent infections, we used it to further analyze whether the response to viral infections may rely on NOD2-associated signaling. Using the macrophage cell-line Raw264.7, we confirmed that MNoV_S99 is able to induce phosphorylation of STAT1 (Tyrosine 701) at different times at Moi 1 (Fig. S2). pSTAT1 was detectable as early as 15 min post-infection and its expression further increased at 30 min and 1 h, while only a slight increase in the STAT1 level was detectable at later time-points. In addition to the STAT1 activation through the Janus kinases JAK1 and Tyk2, we also examined the status of NF κ B activation. For this purpose, pI κ B α levels were quantified from infected cell lysates. Despite basal low-level activation in mock-infected cells, pI κ B α intensity increased slightly at 30 min and 1 h post-infection even if it failed to reach significance. When checking AKT or the MAPK-ERK signaling axes in the same time frame, MNoV_S99 failed to induce any activation of these signaling pathways (Fig. S2). Next, we analyzed the response of BMDM derived from WT or *Nod2*^{-/-} mice that were infected with increasing doses of MNoV_S99 for 30 or 60 min (Figure 3c). STAT1 activation increased over the course of the acute infection in cells derived from WT mice. In contrast, the levels of pSTAT1 were barely detectable in *Nod2*^{-/-} cells at Moi 1. Similarly, with prolonged times of infection (24 h, Moi 0.1) we measured significantly lowered pStat1 levels in MNoV_S99-infected *Nod2*^{-/-} cells in comparison with WT cells (Figure 3d). However, with a higher dose (Moi 5) this lowered phosphorylation of STAT1 in response to MNoV_S99 infection progressively vanished (Figure 3c), suggesting that NOD2-independent alternative mechanisms of action operate when the viral load is too important.

To examine whether the mitochondrial antiviral signaling (MAVS) adaptor protein is required for sensing MNoV_S99, BMDM derived from Mavs-deficient mice were generated. Interestingly, the higher pStat1 levels measured in WT cells (Moi 0.1, 1 h) were

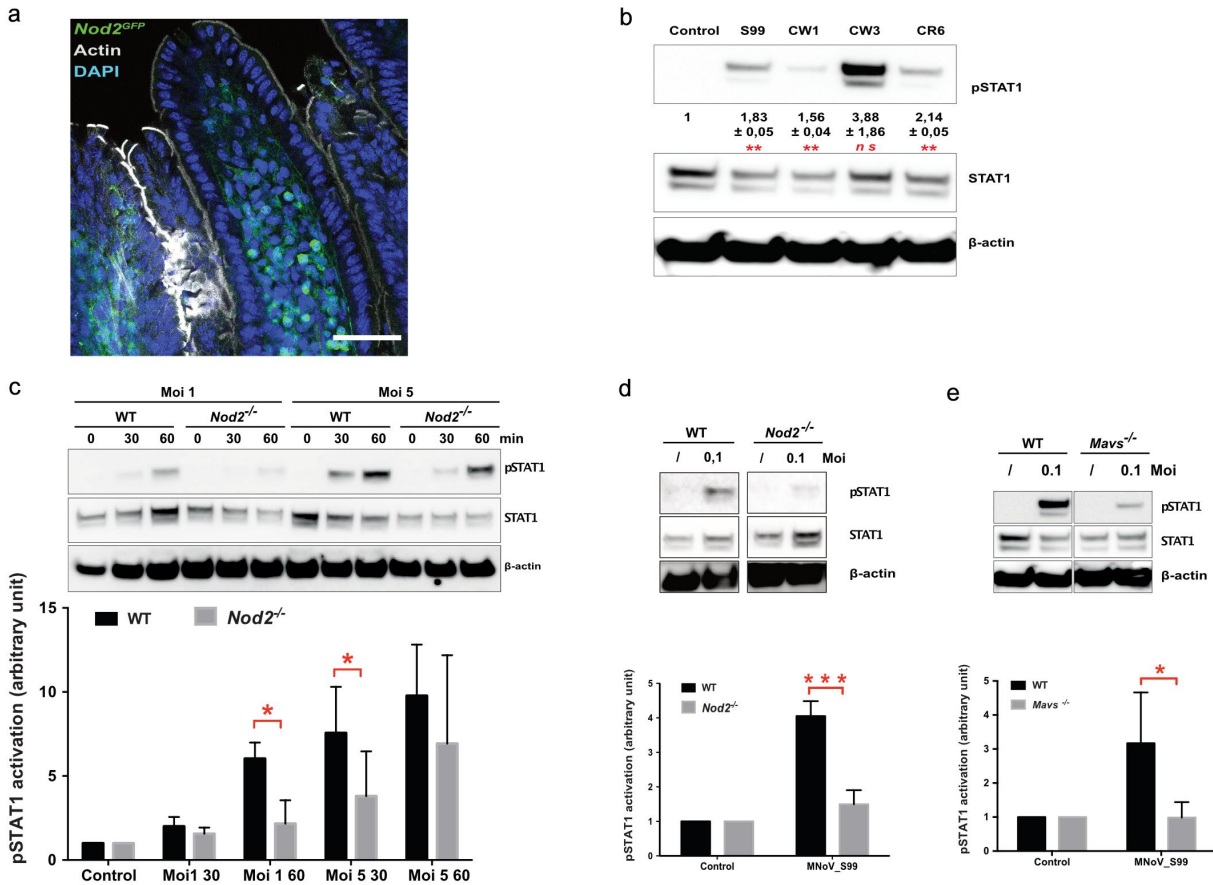


Figure 3. MNoV_S99 associated pro-inflammatory signaling is NOD2 and MAVS-dependent in myeloid lineage cells. a)- Representative image showing an intestinal villus from a *Nod2^{GFP}* mouse. NOD2-GFP is shown in green, actin is stained with Phalloidin in gray and nuclei were stained with DAPI in blue; scale bare represents 50 μ m. b)- Representative western blot showing STAT1 signaling pathway activation after 1 h infection (Moi 1) with the mentioned MNoV strains in BMDM. Below are shown quantification of pSTAT1 bands intensities normalized to β -actin and relative to mock-infected cells ($n = 3$, mean \pm SEM), statistical differences were determined by one-way ANOVA test $*p < 0,05$, $**p < 0,005$. c)- STAT1 activation in response to MNoV_S99 (Moi 1 or 5) in BMDM from WT vs *Nod2^{-/-}* infected for 30 or 60 min. The lower panel shows quantification of pSTAT1, bands intensities normalized to β -actin and relative to mock-infected cells ($n = 3$, mean \pm SEM). Statistical differences were determined by two-way ANOVA test $*p < 0,05$. d)- STAT1 activation in response to MNoV_S99 (Moi 0.1) in WT or *Nod2^{-/-}* BMDM infected for 24 h. Relative quantification of pSTAT1 ($n = 3$, mean \pm SEM) is shown in the lower panel, statistical differences were determined by two-way ANOVA test $***p < 0,0005$. e)- STAT1 activation in response to MNoV_S99 (Moi 0.1) in BMDM from WT vs *Mavs^{-/-}* infected for 60 min. Relative quantification of pSTAT1 ($n = 4$, mean \pm SEM) are shown below. Statistical differences were determined by two-way ANOVA test $*p < 0,05$.

significantly decreased in BMDM from *Mavs^{-/-}* cells (Figure 3e).

Altogether, these data show a mild but significant activation of STAT1 following MNoV_S99 infection in our *in vitro* cellular models. These signaling responses can be at least partially abrogated in the absence of MAVS and NOD2.

Lower levels of inflammation in *Nod2^{-/-}* mice benefit noroviral propagation

MNoV_CR6 infection in DSS-induced colitis was previously shown to promote inflammation in

a functional Atg1611-dependent manner.²¹ Using this viral strain that promotes STAT1 phosphorylation in similar degree than MNoV_S99 (Figure 3b), we checked how loss of *Nod2* influenced resolution of inflammation in response to 3% DSS treatment in mice. As shown with the MNoV_S99 strain, loss of NOD2 improved the muscle thickening of the colon wall in mice infected with MNoV_CR6 (Figure 4a). However, a CR6 strain-specific effect can be observed in these experiments since significantly increased inflammation was only measured in *Atg1611* hypomorph mice but not in WT mice as opposed to MNoV_S99.

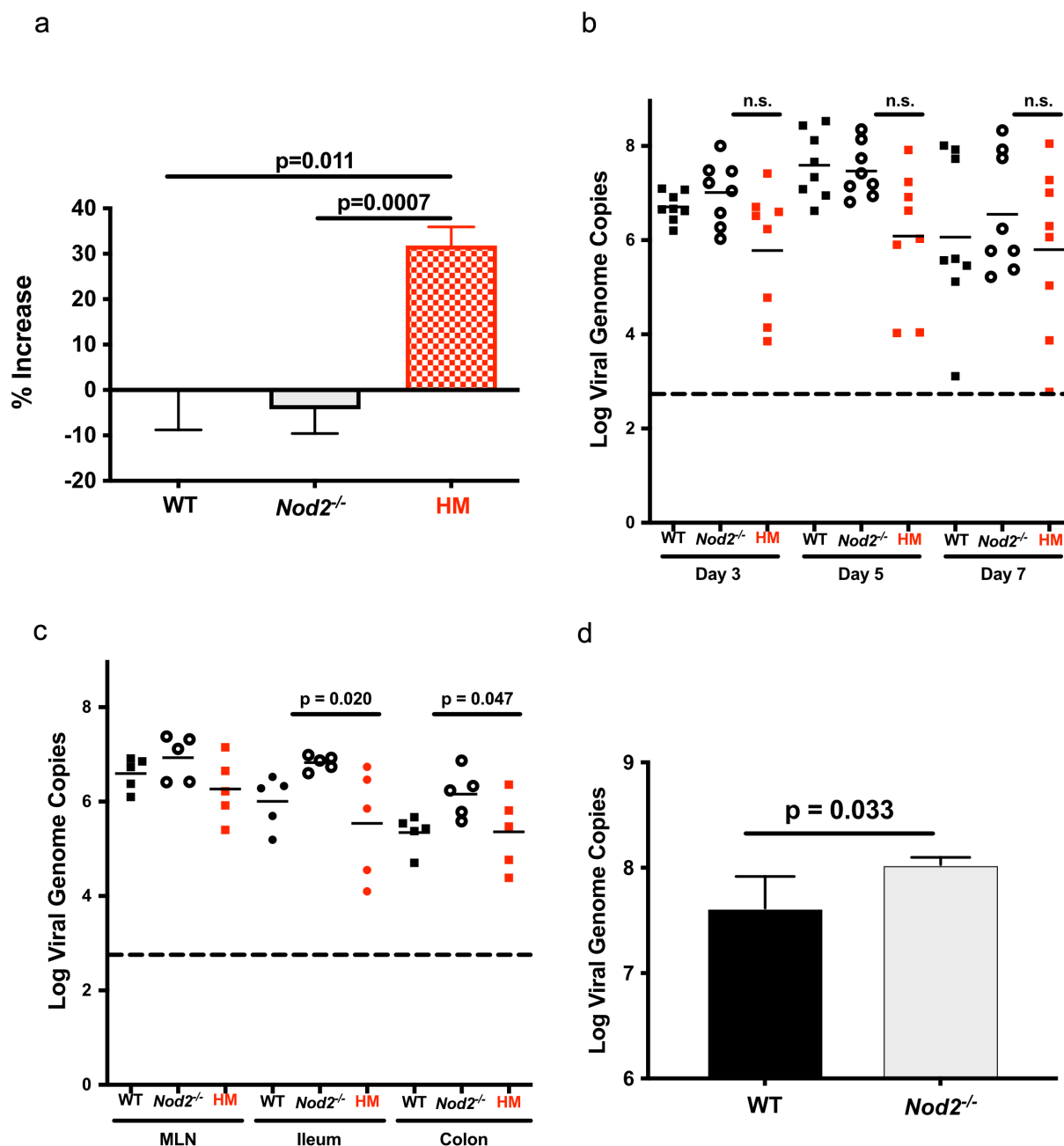


Figure 4. NOD2-dependent noroviral load. a)- WT, *Nod2*^{-/-} and *Atg16l1*^{HM} mice (n = 5 each) were treated with 3% DSS and infected with MNoV_CR6 (3×10^7 PFU). Inflammation was measured as percentage of increase in muscle thickness at the anal-rectal junction in colonic section images plotted after baseline subtraction relatively to the values obtained from WT mice. b)- the viral load measured in stools from WT, *Nod2*^{-/-} and *Atg16l1*^{HM} mice at days 3, 5, and 7 post-infection with MNoV_CR6 (3×10^7 PFU) (n = 8). c)- the viral load measured from indicated tissue samples from MNoV_CR6 infected (3×10^7 PFU) WT, *Nod2*^{-/-} and *Atg16l1*^{HM} mice that were treated for 1 week with DSS 3% (n = 5). d)- MNoV_S99 genome quantification from WT and *Nod2*^{-/-} BMDM cells infected with MNoV_S99 (Moi 0.1 for 24 h) (n = 3). All the statistical differences were measured with Student's *t*-test.

Next, we examined the impact of the pro-inflammatory signaling activation on viral propagation in these mice. In the absence of DSS-induced inflammation, no significant differences could be found when comparing the viral load in the stool of WT, *Atg16l1*^{HM} or *Nod2*^{-/-} mice

(Figure 4b). By contrast, the measured viral load was significantly increased in ileum and colon of DSS-treated *Nod2*^{-/-} mice in comparison with tissues of *Atg16l1*^{HM} mice (Figure 4c). We have also analyzed the viral replication in BMDM derived from WT or *Nod2*^{-/-} mice infected

in vitro with MNoV_S99 (Moi 0.1 for 24 h). In this case, a slight but significant increase in the number of viral genomes was measured from *Nod2*^{-/-} derived cultures (Figure 4d). Hence, the lower levels of inflammation found in *Nod2*^{-/-} mice seem to favor a higher propagation of these two persistent strains.

MNoV_S99 infection promotes bacterial sensing by NOD2

To further explore the mechanisms behind the excessive inflammatory response associated with

noroviral infections, we examined whether noroviral infection may enhance *Nod2* expression levels using RT-qPCR. As what was previously observed with MNoV-1,¹⁵ the transcription level of NOD2 was significantly enhanced in response to MNoV_S99 infection in either Raw264.7 cells or BMDM derived from WT mice (Figures 5a–5b).

This increased *Nod2* expression following norovirus infection could explain at least partially the viral-induced pathogenesis that we observed in our colitis models. Indeed, the greater expression of NOD2 should spike up when suddenly intestinal mononuclear phagocytes interact with intestinal

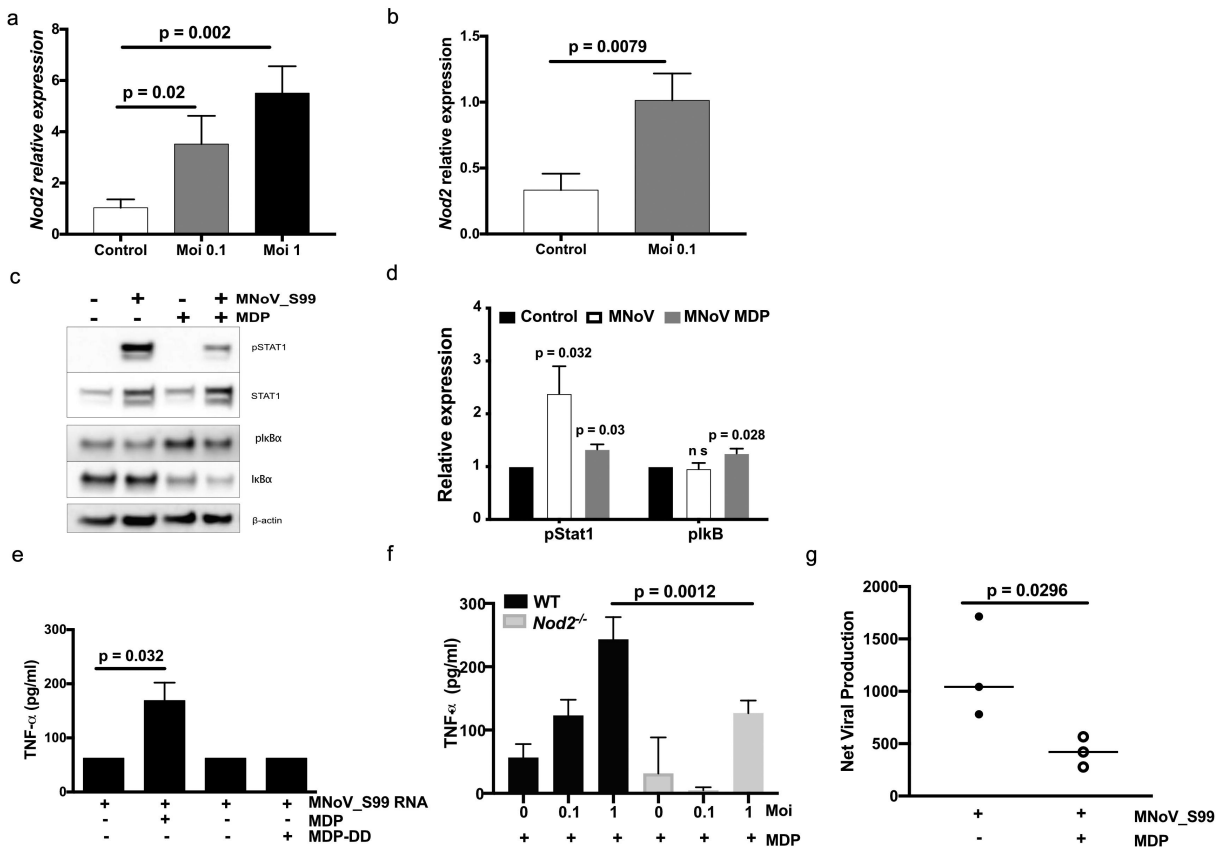


Figure 5. NOD2-dependent pro-inflammatory signaling associated with MNoV_S99 infection and bacterial MDP. Quantification of *Nod2* mRNA levels measured by RT-qPCR in a)- in Raw264.7 cells infected with MNoV_S99 (Moi 0.1 or 1, for 24 h) and in b)- in BMDM from WT mice (Moi 0.1, for 24 h) normalized to *ActB* and relative to mock-infected cells ($n=3$). c)- Representative western blot showing STAT1 and IκBα signaling pathways modulation in cell lysates from monocytes that were either infected with MNoV_S99 (Moi 5, 2 h), treated with MDP (10 ng/mL, 2 h), or a combination of both. d)- quantification and comparison of pSTAT1 and plkBα signals between MNoV_S99 infected alone cells or in combination with MDP (10 ng/mL, 2 h), ($n=3$), with the band intensity being normalized to β-ACTIN and relative to mock-treated cells. e) TNFα production by BMDC subjected to MNoV_S99's ssRNA (10 μg/mL) alone, or supplemented with either MDP (1 μg/mL) or MDP-DD (1 μg/mL) overnight. f) TNFα production by BMDM cells infected with MNoV_S99 (Moi 0.1 or 1) for 6 h, prior to being treated with MDP (10 μg/mL) overnight. g) Net production of MNoV_S99 in Raw264.7 cells infected with MNoV_S99 (Moi 1 for 2 h before MDP treatment (100 ng/mL) for 24 h). Statistical differences were analyzed with Student's t test.

commensal bacteria following DSS-induced epithelial abrasion. We next evaluated whether this heightened expression of NOD2 in response to MNoV_S99 infection may enhance bacterial sensing. While MNoV_S99 infection did induce Stat1 (but not I κ B α) activation in monocytes isolated from WT mice (Figures 5c–5d, MNoV_S99+, MDP- condition), MDP alone triggered potent I κ B α activation without activating Stat1 (Figure 5c, MNoV_S99-, MDP+ condition). Interestingly, MNoV_S99 infection followed by the secondary MDP treatment was associated with significant phosphorylation of both Stat1 and I κ B α (Figure 5d, MNoV_S99+, MDP+ vs mock treated cells). In the same line of investigation, we noticed a significantly augmented pro-inflammatory cytokine TNF α response to MDP in dendritic cells that were first primed with noroviral RNA (Figure 5e). Next, the secretion of TNF α was measured in the supernatants from WT and *Nod2*^{-/-} BMDM cultures infected with MNoV_S99 followed by the MDP treatment. TNF α levels were increased with increasing doses of virus in WT cells, while they remained undetectable (Moi 0.1) or much lower (Moi 1) in *Nod2*^{-/-} cells (Figure 5f). Equally of importance, viral titers measured in supernatants showed significantly decreased yields when infected cells were treated with MDP (Figure 5g).

Overall, these data show that the increased *Nod2* transcription levels following noroviral infections may at least partially promote an inflammatory response to bacterial MDP, leading ultimately to a limitation in the viral propagation. Hence, lowered inflammation in *Nod2*^{-/-} mice is associated with increased dissemination of MNoV_S99 and MNoV_CR6 strains, suggesting that bacterial sensing through NOD2 may regulate their persistence.

Discussion

Intestinal homeostasis is tightly regulated by the interplay between the microorganisms found in the gut microbiota, intestinal epithelial cells, and mononuclear phagocytes. The breach in gut flora homeostasis termed dysbiosis is becoming central to the onset of chronic inflammatory bowel diseases, such as Crohn's disease.^{28,29} With the development of molecular biology techniques, alterations in the virome relevant to disease pathogenesis are thoroughly under investigation.² As such, the role played by

noroviruses was studied in several gastrointestinal inflammatory models. An endemically circulating mouse norovirus strain was shown to promote intestinal barrier dysfunctions and inflammatory lesions caused by loss of tolerance to commensal bacteria in *Il10*^{-/-} mice.³⁰ The secondary challenge with a pathogenic *E. coli* strain following MNoV-1's infection can even cause lethal lesions due to the induction of an unresolved proinflammatory cytokine secretion in a *Nod1/2* dependent manner¹⁹. The hypothesis of an environmental-driver in genetically susceptible hosts that could be at the origin of Crohn's-like disease was also explored with the MNoV_CR6 strain in the *Atg16l1*^{H^M} mice presenting defective autophagy in a DSS colitis model.²¹

NOD2 is very well known for its pathogen-associated molecular pattern recognition activity against bacteria,¹⁷ and recently, it appears it can also participate in the detection of certain viruses.¹⁸ Using pro-inflammatory signaling activation downstream of NOD2 as a read-out, we have analyzed if NOD2 can also participate in MNoV detection and elimination. All our *in vitro* experiments with monocytic lineage derived primary cells (e.g. BMDM, BMDc, BM) and cell lines (e.g. Raw264.7) infected with different MNoV strains showed activation of the STAT1 signaling pathway implicated in the pro-inflammatory IFN and TNF α responses. By contrast, these responses were abrogated in *Nod2*^{-/-} and *Mavs*^{-/-} mice derived from BMDM.

Among enteric viruses commonly found in the microbiota, noroviruses have been proposed to be good candidates in the hypothesis of an environmental-driver in genetically susceptible hosts at the origin of Crohn's disease onset. MNoV_CR6 strain was shown to induce colitis in *Atg16l1*^{H^M} mice presenting defective autophagy in a DSS colitis model.²¹

Several PRRs are implicated in viral sensing. MDA-5 and TLR3 have been shown to participate in the detection of either MNoV_1 or CW3.¹⁵ These are both strains which do not persist *in vivo*, contrary to the S99 (*Berlin*)²⁵ and CR6 that were used in our study.

Our *in vivo* data show significantly exacerbated inflammation when applying either 3% or 5% DSS colitis protocol to WT or *Atg16l1*^{H^M} mice. The excessive MNoV_S99 or MNoV_CR6 associated inflammatory response was abrogated in *Nod2*^{-/-} mice or in BMDM derived from these mice.

Hence, NOD2-dependent signaling adds a layer of regulation to the viral sensing and propagation. While in our norovirus + DSS model knocking-down NOD2 prevents gut inflammation, it has the opposite effect with influenza A virus (IAV) infection in the lung of *Nod2*^{-/-} or *Ripk2*^{-/-} mice.³¹ Indeed, the NOD2-RIPK2 signaling axis has been shown to downmodulate the NLRP3-dependent mitophagy activation and the associated inflammatory response in the lung tissue of infected mice.

Norovirus propagation or prolonged persistence is tightly regulated by the interplay between several signaling pathways. MNoV_1 replication was shown to be inhibited in macrophages following LPS mediated NF- κ B activation that in turn triggers IFN- β -dependent JAK-STAT antiviral activity.³² Interestingly, in our cellular models, in addition to the phosphorylation of STAT1 that we observed when cells were infected with MNoV_S99, the heightened *Nod2* expression levels preceded a greater ability of cells to respond to bacterial MDP. Consequently, the subsequent treatment with MDP induced an increased Nf κ B signaling pathway via I κ B α activation. The sequential activation of these two pro-inflammatory signaling pathways resulted in the inhibition of the MNoV_S99 propagation on the one hand and the augmented production of the pro-inflammatory cytokine TNF α in response to MDP on the other hand. Hence, the aggravated inflammatory pathology we observed in our DSS colitis model can be explained by this NOD2-dependent signaling loop in MNoV_S99 or MNoV_CR6 infected mice.

In conclusion, our study shows a NOD2-dependent bacterial sensing that prevents dissemination of the persistent MNoV_S99 and MNoV_CR6 strains.

Methods

Unless otherwise indicated, all media and reagents were purchased from Thermo Fischer Scientific.

Colitis mouse model and viral infection

All animal experiments were approved by the local ethical committee n° CEEA - 2016030717519,903. Age and gender-related *Nod2*^{-/-} and wild-type C57BL/6J mice (CDTA, Orléans, France) were

housed four to six per cage, under a strict pathogen-free environment. Mice were gavaged with 5×10^7 TCID₅₀/mL of MNoV_S99 diluted in 200 μ L PBS or mock treated with PBS only. 7 d post-infection, drinking water was substituted with a 3–5% dextran sodium sulfate (DSS) (35,000–40,000 MW; TdB Consultancy) solution replaced every 2 d for a total duration of 7 d. 3% DSS colitis experiments with MNoV_CR6 were conducted as previously described in.²¹

Cells and virus

Mouse leukemic monocyte macrophage cell line RAW264.7 were purchased from ECCAC (Sigma-Aldrich) and maintained in Dulbecco's modified Eagle's medium (DMEM), supplemented with 10% (*v/v*) fetal bovine serum, 1% penicillin/streptomycin, and 1% sodium pyruvate.

Bone marrow-derived macrophages (BMDMs) were isolated from femurs of wild-type, *Nod2*^{-/-}, or *Mavs*^{-/-} mice of C57BL/6J background.³³ Using a 26 G $\frac{1}{2}$ " needle, bone marrow cells were flushed out of the bones with Iscove's modified Dulbecco's medium (IMDM), supplemented with 10% fetal bovine serum, 1% penicillin/streptomycin, 1% non-essential amino acid, 1% sodium pyruvate, 1% glutamine, and 20% (*v/v*) conditioned-media from L929 cells. Red blood cells were lysed using a 160 mM NH₄CL and 170 mM Tris solution for 5 min at RT. 3 to 6×10^6 viable cells were plated in non-cell-culture-treated petri dishes and grown for 5–7 d in the above mentioned fully supplemented IMDM medium.

Bone marrow-derived dendritic cells were isolated similarly as BMDM cells. Then, 2×10^6 viable cells were plated in non-cell-culture-treated petri dishes and grown for 7 d in RPMI 1640, supplemented with 10% fetal bovine serum, 1% penicillin/streptomycin, 1% L-glutamine, 1% HEPES, and 20% (*v/v*) conditioned-media from J558 cell line producing murine granulocyte monocyte colony stimulating factor (GM-CSF).

Monocytes were isolated from bone marrow cells by using the mouse Monocyte Isolation Kit (Miltenyi Biotec) and a QuadroMACS separator.

The MNoV_S99 strain (GenBank accession no. DQ911368) was provided by Prof. P. Maris from ANSES Fougères Laboratory (France) and was propagated in RAW 264.7 cells. MNoV_CR6

concentrated stocks were prepared as described in.³⁴ Briefly, supernatant from 293T cells transfected with a plasmid containing the viral genome was applied to RAW264.7 cells to amplify virus production, and virions were concentrated by ultracentrifugation and resuspension in endotoxin-free PBS. Concentration of stocks was determined by plaque assay.

For *in vitro* infection experiments, $3\text{--}5 \times 10^5$ viable cells were seeded in six well plates. The next day, just before viral infection, cells were counted from one well to determine precisely the multiplicity of infection (Moi). In the remaining wells medium was removed and replaced with variable quantities of MNoV_S99 from a common viral stock in a final volume of 1 mL fresh medium per well. Mock treated cells were incubated in parallel with matching quantities of culture media from non-infected cells that were generated at the same time as viral stocks.

At various time-points after infection, supernatant was removed and cells were washed once with PBS, before lysis in RIPA buffer for WB analysis or RLT buffer for total RNA extraction (RNAeasy kit, Qiagen) for RT-qPCR experiments.

Immunohistochemistry, ELISA, western blot, RT-qPCR, and titration

For immunohistochemistry analysis, formalin-fixed colon samples were embedded in paraffin. 5 μm sections were stained with H&E. Slides were imaged with an AxioPlan 2 (Zeiss) microscope and blindly scored for inflammation severity by two investigators as previously described.³⁵ Briefly, tissue lesions were scored from 0 to 3, so was the infiltration of inflammatory cells in the lamina propria. A combined score was calculated, ranging from 0 (no changes) to 6 (wide-spread cellular infiltrations and extensive tissue damage).

The muscularis propria thickness was measured from light microscopy images of H&E stained colon sections using Image J (NCBI). Five measurements from different locations were performed for each animal and compared with colon sections from mock treated animals.

For ELISA analysis, briefly 1 cm colon samples were recovered from mice, luminal content was flushed with PBS, samples were cut opened and resuspended overnight in 250 μl DMEM

supplemented with 1% penicillin/streptomycin in 24 well plate at 37°C. The following day, supernatants were collected and stored at -80°C before cytokine measurement. TNF α and Interleukin-6 protein levels were measured specifically using pre-coated 96 well ELISA plates (R&D System) following manufacturers' indications.

For TNF α ELISA from BMDC, 5×10^5 cells were plated in 24 well plates and treated with MNoV_S99's ssRNA (extracted with RNeasy Qiagen kit) with Lipofectamine 2000¹⁸ \pm MDP or MDP-DD (Invivogen) overnight and supernatants were measured for TNF α levels.

For TNF α ELISA from BMDM, 2×10^5 cells were plated in 96 well plates infected with MNoV_S99 (Moi 0.1 or 1) for 6 h prior to MDP treatment (10 $\mu\text{g}/\text{mL}$) overnight, and supernatants were measured for TNF α levels.

For western blot analysis, total proteins from cell lysates were quantified by BCA protein assay kit (Pierce), equalized amounts of proteins (10–20 μg) were resolved by 4–15% gradient SDS-PAGE gels and transferred to nitrocellulose membranes. Membranes were blocked in 0.05% PBS-Tween, 5% skimmed milk solution, before incubation subsequently with primary and secondary antibodies diluted (see Table 1) in a blocking solution. Following secondary antibodies incubations, signals of interest were detected using a chemiluminescence reader (ImageQuantTM Las 4000, GE Healthcare Life Sciences), images were processed, and band ROIs were quantified with Image J software (NCBI). The mean band intensities \pm SDs of protein of interest were normalized to β -ACTIN. Relative values to control mock-infected conditions were compared between different experiments.

For *Nod2* quantification from MNoV_S99 infected BMDM or RAW264.7 cells, total RNA extraction was performed using the RNeasy Mini Kit (Qiagen). One μg of RNA was reversed transcribed in the presence of 2.5 mM of oligo-dT using the Reverse Transcription kit (Roche) following the manufacturer's instructions. 75 ng of cDNAs were used for the qPCR analyses using Q5 High-Fidelity 2X Master Mix (New England BioLabs). *Nod2* and *Actb* were specifically amplified using the Fwd_5'GGAAACAACATTGGCAGCA T3' and Rev_5'TCTTGAGTCCTTCTGCGAGA3' Fwd_5'TTCTTTGCAGCTCCTTCGTT3' and Rev_5'ATGGAGGGGAATACAGCCC3', respectively. Ac

Table 1. Antibodies used for western blotting.

	Dilution	Supplier
Primary antibodies		
anti-phosphoSTAT1 (Tyr 701) (58D6) (85kDa)	1/1000	Cell Signaling Technology
anti-STAT1(D1K9Y)(85kDa)	1/1000	
anti-phospholkbA (Ser32/36) (5A5) (40kDa)	1/1000	
anti-IkBα (44D4) (39kDa)	1/1000	
anti-phosphoAKT (Ser473) (D9E) (60kDa)	1/1000	
anti-AKT (60kDa)	1/1000	
anti-phospho44/42 MAPK (Erk1/2) (Trh202/Tyr204) (197G2) (42, 44 kDa)	1/1000	
anti-p44/42 (Erk1/2) (42, 44 kDa)	1/1000	
anti-β-ACTIN (45kDa)	1/500	
Secondary antibodies		
anti-Rabbit_HRP (#711-035-152)	1/5000	Jackson Laboratories
anti-Mouse_HRP (#115-005-003)	1/5000	

tb was used as an internal reference gene in order to normalize the transcript levels. The relative mRNA levels ($2^{-\Delta\Delta Ct}$) were determined by comparing (a) the PCR cycle thresholds (Ct) for *Nod2* and *Actb* (ΔCt) and (b) ΔCt values for treated and control groups ($\Delta\Delta Ct$).

MNoV_S99 load was determined by measuring the MNoV genome copy numbers using RT-qPCR analysis as previously described³⁶. Briefly, total RNA was extracted from BMDM cell cultures using the RNeasy Mini Kit (Qiagen). 5 μ L of RNA were used per reaction of RT-qPCR. Viral genome levels were determined using the Takyon™ Dry No Rox One-Step RT Probe Mastermix (Eurogentec). Viral genomes were specifically amplified using the Fwd_5'GTGCGCAACACAGAGAAAACG3' and Rev_5'CGGGCTGAGCTTCCTGC3' primers that target the MNoV ORF1 region combined with the TaqMan probe 5'[6-FAM]-CTAGTGTCTCCTTTGGAGCACCTA-[BHQ1]3' using the Strata gene Mx3005P (Agilent Technologies) with 1 RT cycle and 40 cDNA amplification cycles. The quantification of viral genome copies was obtained using a standard curve (ranging from 2×10^1 to 2×10^6 genome copies) with serial dilutions of the plasmid pMNoV1 corresponding to the full genome of MNoV_1 (Dr Christiane Wobus, University of Michigan, USA). Viral load for MNoV_CR6 strain was determined by measuring genome copy numbers using RT-qPCR analysis as previously described in²¹.

The net production of MNoV_S99 was determined using the TCID50 method as described in³⁵. Briefly, Raw264.7 cells were infected at *Moi* 1 with MNoV_S99 for 2 h, before adding MDP (100 ng/mL) or not in the supernatant for

24 h. Titers ($n = 3$) were obtained from each supernatant. The net production is calculated by normalizing the amount of viruses produced with the amount of viruses used for the infection.

***NOD2*^{GFP} immunohistochemistry imaging**

NOD2^{GFP} mice³⁷ in the C57BL/6 background were maintained at the Institut Pasteur Central Animal facility. We used heterozygous *NOD2*^{GFP} mice since the presence of one functional copy of *NOD2* ensures that physiological responses dependent on functional *NOD2* are not impaired. Heterozygous *NOD2*^{GFP} female mice (8–12 weeks of age) were sacrificed, and several centimeters of the distal ileum were removed, opened longitudinally, and washed in PBS. The tissue was spread flat over a 4% *w/v* LMP agarose (Merck) pad and fixed with 4% *v/v* paraformaldehyde (VWR). The ileal tissue was then embedded in a 4% LMP agarose block and cut into 200 μ m-thick sections using a Microm HM 650 V Vibration microtome.

For staining, tissues were blocked and permeabilized overnight in a solution containing 0.4% Triton X-100 (Merck) and marked with an anti-GFP (rabbit polyclonal antibody A-11122, Invitrogen) primary antibody and secondary Alexa Fluor 488 goat anti-rabbit antibody (Invitrogen). Tissue sections were counterstained with DAPI (1 μ g/mL, BD Biosciences) and Phalloidin-iFluor 647 (1:200 dilution, Abcam) and mounted using ProLong Gold Antifade reagent. Confocal acquisitions were performed using a Leica HyD SP5 confocal

microscope. Image analysis was performed using Icy version 2.4.2.0.³⁸

Acknowledgments

We thank the UTechS PBI for the *NOD^{GFP}* tissue imaging assistance. We thank the members of the Institut Pasteur Central Animal Facility for their assistance with animal studies. We thank T. Durand and MP. Fourmaux for excellent technical assistance.

Disclosure statement

K.C. has received research support from Pfizer, Takeda, Pacific Biosciences, Genentech, and AbbVie; consulted for or received honoraria from Vedanta, Genentech, and AbbVie; and holds U.S. patent 10,722,600 and provisional patent 62/935,035 and 63/157,225.

Funding

The UTechS PBI, a member of the France - BioImaging infrastructure network was supported by the French National Research Agency Investissement d'Avenir program (ANR-10-INSB-04). I.G.B. laboratory was supported by Laboratoire d'Excellence "Integrative Biology of Emerging Infectious Diseases" initiative of the Investissement d'Avenir program (ANR-10-LABX-62-IBEID), the RHU Torino Lumière initiative of the Investissement d'Avenir program (ANR-16-RHUS-0008), the French National Research Agency (ANR-16-CE15-0021) and R&D grants from Danone and MEIJI. M.C. was supported by grants from the Fondation pour la Recherche Médicale (DEQ20130326475) and the European Union's European Regional Development fund.

ORCID

Ghaffar Muharram  <http://orcid.org/0000-0003-4309-8450>

Authors' contribution

G.M. and M.T. performed the majority of the experimental procedures. T.G. contributed to the preclinical studies in mice. M.D., T.G., and O.B. performed RT-qPCR and ELISA analysis. M.D. contributed to histological analysis of colon sections. E.W. performed viral genome quantification using RT-qPCR. R.W. and I.G.B. performed a histological analysis of tissue sections from NOD2- β -Gal reporter mice. All authors contributed to the interpretation of the raw data and

critically reviewed and/or modified the manuscript. G.M. and M.C. conceived, designed, and wrote the paper.

Data availability statement

The data that support the findings of this study are available from the corresponding authors, GM and MC, upon request on HAL. <https://hal.science/hal-04101382>.

References

1. Cadwell K, Pfeiffer J. Expanding the role of the virome: commensalism in the gut. *J Virol*. 2015;89(4):1951–1953. doi:10.1128/JVI.02966-14.
2. Norman JM, Handley S, Baldridge M, Droit L, Liu C, Keller B, Kambal A, Monaco C, Zhao G, Fleshner P, et al. Disease-specific alterations in the enteric virome in inflammatory bowel disease. *Cell*. 2015;160(3):447–460. doi: 10.1016/j.cell.2015.01.002.
3. Pfeiffer JK, Virgin HW. Viral immunity. Transkingdom control of viral infection and immunity in the mammalian intestine. *Sci*. 2016;351(6270):aad5872. doi:10.1126/science.aad5872.
4. Ettayebi K, Crawford SE, Murakami K, Broughman JR, Karandikar U, Tenge VR, Neill FH, Blutt SE, Zeng X-L, Qu L, et al. Replication of human noroviruses in stem cell-derived human enteroids. *Sci*. 2016;353(6306):1387–1393. doi: 10.1126/science.aaf5211.
5. Estes MK, Ettayebi K, Tenge VR, Murakami K, Karandikar U, Lin S-C, Ayyar BV, Cortes-Penfield NW, Haga K, Neill FH, et al. Human norovirus cultivation in nontransformed stem cell-derived human intestinal enteroid cultures: Success and challenges. *Viruses*. 2019;11(7):E638. doi: 10.3390/v11070638.
6. Ludwig-Begall LF, Mauroy A, Thiry E. Noroviruses—the state of the art, nearly fifty years after their initial discovery. *Viruses*. 2021;13(8):1541. doi:10.3390/v13081541.
7. Newman KL, Leon JS. Norovirus immunology: Of mice and mechanisms. *Eur J Immunol*. 2015;45(10):2742–2757. doi:10.1002/eji.201545512.
8. Wobus CE, Karst SM, Thackray LB, Chang K-O, Sosnovtsev SV, Belliot G, Krug A, Mackenzie JM, Green KY, Virgin HW, et al. Replication of norovirus in cell culture reveals a tropism for dendritic cells and macrophages. *PLoS Biol*. 2004;2(12):e432. doi: 10.1371/journal.pbio.0020432.
9. Thackray LB, Wobus CE, Chachu KA, Liu B, Alegre ER, Henderson KS, Kelley ST, Virgin HW. Murine noroviruses comprising a single genogroup exhibit biological diversity despite limited sequence divergence. *J Virol*. 2007;81(19):10460–10473. doi:10.1128/JVI.00783-07.

10. Nice TJ, Strong DW, McCune BT, Pohl CS, Virgin HW. A single- amino-acid change in murine norovirus NS1/2 is sufficient for colonic tropism and persistence. *J Virol.* 2013;87(1):327–334. doi:10.1128/JVI.01864-12.
11. Nice TJ, Baldridge MT, McCune BT, Norman JM, Lazear HM, Artyomov M, Diamond MS, Virgin HW. Interferon- λ cures persistent murine norovirus infection in the absence of adaptive immunity. *Sci.* 2015;347(6219):269–273. doi:10.1126/science.1258100.
12. Karst SM, Wobus CE, Lay M, Davidson J, Virgin HW. STAT1-dependent innate immunity to a Norwalk-like virus. *Sci.* 2003;299(5612):1575–1578. doi:10.1126/science.1077905.
13. Hwang S, Maloney N, Bruinsma M, Goel G, Duan E, Zhang L, Shrestha B, Diamond M, Dani A, Sosnovtsev S, et al. Nondegradative role of Atg5-Atg12/Atg16L1 autophagy protein complex in antiviral activity of interferon gamma. *Cell Host & Microbe.* 2012;11(4):397–409. doi: 10.1016/j.chom.2012.03.002.
14. Thorne LG, Goodfellow IG. Norovirus gene expression and replication. *J Gen Virol.* 2014;95(2):278–291. doi:10.1099/vir.0.059634-0.
15. McCartney SA, Thackray LB, Gitlin L, Gilfillan S, Virgin IV HW, Colonna M. MDA-5 recognition of a murine norovirus. *PLoS Pathog.* 2008;4(7):e1000108. doi:10.1371/journal.ppat.1000108.
16. Wang P, Zhu S, Yang L, Cui S, Pan W, Jackson R, Zheng Y, Rongvaux A, Sun Q, Yang G, et al. Nlrp6 regulates intestinal antiviral innate immunity. *Sci.* 2015;350(6262):826–830. doi: 10.1126/science.aab3145.
17. Chamillard M, Girardin SE, Viala J, Philpott DJN. Nods, Nalps and Naip: intracellular regulators of bacterial-induced inflammation. *Cell Microbiol.* 2003;5(9):581–592. doi:10.1046/j.1462-5822.2003.00304.x.
18. Sabbah A, Chang TH, Harnack R, Frohlich V, Tominaga K, Dube PH, Xiang Y, Bose S. Activation of innate immune antiviral responses by Nod2. *Nat Immunol.* 2009;10(10):1073–1080. doi:10.1038/ni.1782.
19. Kim Y-G, Park J-H, Reimer T, Baker D, Kawai T, Kumar H, Akira S, Wobus C, Núñez G. Viral infection augments Nod1/2 signaling to potentiate lethality associated with secondary bacterial infections. *Cell Host & Microbe.* 2011;9(6):496–507. doi:10.1016/j.chom.2011.05.006.
20. Mumphrey SM, Changotra H, Moore TN, Heimann-Nichols ER, Wobus CE, Reilly MJ, Moghadamfalahi M, Shukla D, Karst SM. Murine norovirus 1 infection is associated with histopathological changes in immunocompetent hosts, but clinical disease is prevented by STAT1-dependent interferon responses. *J Virol.* 2007;81(7):3251–3263. doi:10.1128/JVI.02096-06.
21. Cadwell K, et al. Virus-plus-susceptibility gene interaction determines Crohn's disease gene Atg16L1 phenotypes in intestine. *Cell.* 2010;141:1135–1145. doi:10.1016/j.cell.2010.05.009.
22. Travassos LH, Carneiro LAM, Ramjeet M, Hussey S, Kim Y-G, Magalhães JG, Yuan L, Soares F, Chea E, Le Bourhis L, et al. Nod1 and Nod2 direct autophagy by recruiting ATG16L1 to the plasma membrane at the site of bacterial entry. *Nat Immunol.* 2010;11(1):55–62. doi: 10.1038/ni.1823.
23. Hugot JP, et al. Association of NOD2 leucine-rich repeat variants with susceptibility to Crohn's disease. *Nature.* 2001;411:599–603. doi:10.1038/35079107.
24. Hampe J, Franke A, Rosenstiel P, Till A, Teuber M, Huse K, Albrecht M, Mayr G, De La Vega FM, Briggs J, et al. A genome-wide association scan of nonsynonymous SNPs identifies a susceptibility variant for Crohn disease in ATG16L1. *Nat Genet.* 2007;39(2):207–211. doi: 10.1038/ng1954.
25. Niendorf S, Klemm U, Mas Marques A, Bock C-T, Höhne M, Boon AC. Infection with the persistent murine norovirus strain MNV-S99 suppresses IFN-Beta release and activation of Stat1 in vitro. *PLoS One.* 2016;11(6):e0156898. doi:10.1371/journal.pone.0156898.
26. Hrdý J, Alard J, Couturier-Maillard A, Boulard O, Boutillier D, Delacre M, Lapadatescu C, Cesaro A, Blanc P, Pot B, et al. Lactobacillus reuteri 5454 and Bifidobacterium animalis ssp. lactis 5764 improve colitis while differentially impacting dendritic cells maturation and antimicrobial responses. *Sci Rep.* 2020;10(1):5345. doi: 10.1038/s41598-020-62161-1.
27. Wilen CB, Lee S, Hsieh LL, Orchard RC, Desai C, Hykes BL, McAllaster MR, Balce DR, Feehley T, Brestoff JR, et al. Tropism for tuft cells determines immune promotion of norovirus pathogenesis. *Sci.* 2018;360(6385):204–208. doi: 10.1126/science.aar3799.
28. Hold GL, Smith M, Grange C, Watt ER, El-Omar EM, Mukhopadhyay I. Role of the gut microbiota in inflammatory bowel disease pathogenesis: what have we learnt in the past 10 years? *World J Gastroenterol.* 2014;20(5):1192–1210. doi: 10.3748/wjg.v20.i5.1192.
29. Kim DH, Cheon JH. Pathogenesis of inflammatory bowel disease and recent advances in biologic therapies. *Immune Netw.* 2017;17(1):25–40. doi:10.4110/in.2017.17.1.25.
30. Basic M, Keubler LM, Buettner M, Achard M, Breves G, Schröder B, Smoczek A, Jörns A, Wedekind D, Zschemisch NH, et al. Norovirus triggered microbiota-driven mucosal inflammation in interleukin 10-deficient mice. *Inflamm Bowel Dis.* 2014;20(3):431–443. doi: 10.1097/01.MIB.0000441346.86827.ed.
31. Lupfer C, Thomas PG, Anand PK, Vogel P, Milasta S, Martinez J, Huang G, Green M, Kundu M, Chi H, et al. Receptor interacting protein kinase 2-mediated mitophagy regulates inflammasome activation during virus infection. *Nat Immunol.* 2013;14(5):480–488. doi: 10.1038/ni.2563.
32. Yu P, Li Y, Wang Y, Peppelenbosch MP, Pan Q. Lipopolysaccharide restricts murine norovirus infection

- in macrophages mainly through NF- κ B and JAK-STAT signaling pathway. *Virology*. 2020;546:109–121. doi:10.1016/j.virol.2020.04.010.
33. Michallet M-C, Meylan E, Ermolaeva MA, Vazquez J, Rebsamen M, Curran J, Poeck H, Bscheider M, Hartmann G, König M, et al. TRADD protein is an essential component of the RIG-like helicase antiviral pathway. *Immunity*. 2008;28(5):651–661. doi: 10.1016/j.immuni.2008.03.013.
 34. Kernbauer E, Ding Y, Cadwell K. An enteric virus can replace the beneficial function of commensal bacteria. *Nature*. 2014;516(7529):94–98. doi:10.1038/nature13960.
 35. Hwang S, Alhatlani B, Arias A, Caddy SL, Christodoulou C, Bragazzi Cunha J, Emmott E, Gonzalez-Hernandez M, Kolawole A, Lu J, et al. Murine norovirus: propagation, quantification, and genetic manipulation. *Curr Protoc Microbiol*. 2014;33(1):15K.2.1–61. doi: 10.1002/9780471729259.mc15k02s33.
 36. Wirtz S, Popp V, Kindermann M, Gerlach K, Weigmann B, Fichtner-Feigl S, Neurath MF. Chemically induced mouse models of acute and chronic intestinal inflammation. *Nat Protoc*. 2017;12(7):1295–1309. doi:10.1038/nprot.2017.044.
 37. Barreau F, Meinzer U, Chareyre F, Berrebi D, Niwa-Kawakita M, Dussallant M, Foligne B, Ollendorff V, Heyman M, Bonacorsi S, et al. CARD15/NOD2 is required for Peyer's patches homeostasis in mice. *PLoS One*. 2007;2(6):e523. doi: 10.1371/journal.pone.0000523.
 38. de Chaumont F, Dallongeville S, Chenouard N, Hervé N, Pop S, Provoost T, Meas-Yedid V, Pankajakshan P, Lecomte T, Le Montagner Y, et al. Icy: an open bioimage informatics platform for extended reproducible research. *Nat Methods*. 2012;9(7):690–696. doi: 10.1038/nmeth.2075.